optica

Intense quasi-monochromatic resonant harmonic generation in the multiphoton ionization regime

Mangaljit Singh,[1] Muhammad Ashiq Fareed,[2] Vasily Strelkov,[3,4] Alexei N. Grum-Grzhimailo,[5] Alexander Magunov,[3,6] Antoine Laramée,[1] François Légaré,[1] and Tsuneyuki Ozaki[1,*]

[1]Institut National de la Recherche Scientifique–Énergie Matériaux Télécommunications, 1650 Lionel-Boulet, Varennes, Québec J3X 1S2, Canada
[2]Chemical Sciences Division, Lawrence Berkeley National Laboratory, Berkeley, California 94720, USA
[3]Prokhorov General Physics Institute of the Russian Academy of Sciences, Vavilova Street, 38, Moscow 119991, Russia
[4]Moscow Institute of Physics and Technology (National Research University), 9 Institutskiy per., Dolgoprudny, Moscow Region 141701, Russia
[5]Skobeltsyn Institute of Nuclear Physics, Lomonosov Moscow State University, Moscow 119991, Russia
[6]National Research Institute for Physical-Technical and Radiotechnical Measurements, Mendeleevo, Moscow Region 141570, Russia
*Corresponding author: ozaki@emt.inrs.ca

Received 15 June 2021; revised 17 July 2021; accepted 19 July 2021 (Doc. ID 434185); published 17 August 2021

Resonant high-order harmonics, which result in quasi-monochromatic extreme ultraviolet light with coherent intensity enhancement involving autoionizing resonances, have been demonstrated from laser-ablated plumes in the tunnel-ionization regime. Here, we demonstrate resonant harmonics in the previously unexplored multiphoton-ionization regime. We demonstrate an intense resonant harmonic from gallium with an intensity enhancement ratio of 714 relative to the neighboring harmonics, achieved without the need for extreme ultraviolet filtering methods, thus preventing a typical photon flux loss of more than 70%. Three-dimensional time-dependent Schrödinger equation calculations reveal that this increase in the enhancement ratio is due to the low electron wave packet spreading in the multiphoton-ionization regime. These results reveal a method for increasing the intensity and monochromaticity of intense multimicrojoule femtosecond extreme ultraviolet light and will also facilitate understanding of the involvement of autoionizing resonances in generating resonant harmonics in the multiphoton-ionization regime.

https://doi.org/10.1364/OPTICA.434185

High-order harmonic generation (HHG) is an excellent source of coherent femtosecond (fs) pulses of extreme ultraviolet (XUV) and soft x-ray radiation. HHG takes place when a high-intensity ultrashort laser pulse interacts with a nonlinear media, typically a gas or a laser-ablated plume (LAP) containing atomic or ionic species [1,2]. The mechanism of HHG from most species is explained by the three-step model based on the phenomenon of tunnel-ionization (TI) [3]. The three steps involve the TI of valence electron, its acceleration within the continuum, followed by a radiative transition into the initial ground state emitting the XUV [3]. HHG is a powerful method to study the electronic and structural dynamics of atoms and molecules with fs temporal resolution [4,5]. The harmonic spectrum from a typical noble gas is broadband, containing high-order harmonic series. However, many applications require intense quasi-monochromatic (QM)-XUV pulses, such as XUV pump-probe spectroscopy [6], XUV diffractive imaging [7], and time-resolved photoemission spectroscopy (angle-resolved photoemission spectroscopy (ARPES) and photoemission electron microscopy (PEEM)) [8,9]. The intense QM-XUV sources are also important because they are central to the scientific domain of XUV nonlinear optics investigating the nonlinear laser–matter interactions in the XUV, such as high charge state production through the multi-XUV-photon absorption in noble gases [10,11].

The traditional QM-XUV sources used by the scientific community are the synchrotron-based XUV sources and the XUV free-electron lasers (FELs) [12]. Synchrotron sources produce XUV pulses typically with a duration of a few tens of picoseconds. This long time scale renders synchrotron radiation ineffective for studies requiring fs time-scale resolution. Although complex beam manipulation techniques when integrated into a synchrotron facility could generate 100 fs radiation, the added complexity and the financial expenses associated with the construction and maintenance of a synchrotron facility leave many researchers with the lack of access to such an exotic light source [13,14]. FELs, on the other hand, can produce fs XUV pulses with several microjoules of QM-XUV pulse energies, but the access to this giant multimillion-dollar facility is also limited to a few groups of scientists [12].

HHG is an alternative lab-scale tabletop source of coherent fs XUV radiation [1,2]. However, today, the majority of HHG experiments performed using Ti:sapphire 800 nm fs lasers and long mid-infrared fs lasers have laser parameters satisfying the TI regime of the Keldysh theory [2,15], and hence involve laser–matter interaction in the TI regime [1]. The Keldysh parameter is defined as $\gamma = \sqrt{I_p/2U_p} = 0.231\sqrt{I_p/I\lambda^2}$ (where I_p is the ionization energy in eV, I is the laser intensity in units of 10^{14} W/cm^2, λ is the laser wavelength in μm, and U_p is the ponderomotive energy in eV, which is defined as the cycle average kinetic energy of an electron, and is given by $U_p = 9.34I\lambda^2$). The Keldysh parameter categorizes the laser–matter interaction broadly into two regimes:

multiphoton ionization (MPI) regime for $\gamma > 1$ and TI regime for $\gamma < 1$. Therefore, the TI regime implies a large U_p compared to the I_p and vice versa for MPI. One significant feature of HHG in the TI regime is the generation of a long plateau of high-order harmonics, and hence a very broadband XUV emission. This is a critical issue for the HHG-based sources that need to be employed for experiments requiring intense fs QM-XUV radiation, and therefore is a hurdle that needs to be solved to advance the field of intense laser–matter interactions based on the intense tabletop lab-scale XUV sources. The traditional approach to tackling this issue is to extract a single harmonic order from the broadband harmonic spectrum using XUV optics, for example, a grazing incidence grating monochromator [16]. This results in the reduction of harmonic flux due to the finite diffraction efficiency of the grating monochromator (typical loss > 70%) [16]. The low HHG conversion efficiency is another critical issue (typically 10^{-6}–10^{-7}), generating harmonic energy per pulse at the nanojoule scale [17]. To overcome these obstacles, an alternative and promising XUV source is the QM resonant harmonic (RH) generation from the LAP with a high conversion efficiency of 10^{-4} [2]. A suitable LAP source can generate an intense microjoule-level single XUV RH with an order of magnitude enhancement ratio (ER) relative to the neighboring harmonics [18]. The LAP technique can generate stable harmonics for several minutes at kilohertz-level repetition rates by using rotating cylindrically shaped ablation targets [19,20]. Although microjoule-level harmonic energies have also been demonstrated from gases, such experiments are complicated to implement. They either require several meters long loose-focusing geometries to generate a large laser interaction volume in the gas, or the intricate process of employing multiple gas jets along with careful optimization of nonlinear media configuration to achieve the higher XUV conversion efficiency [10,21].

Since the experiments generating QM-XUV from RH in LAPs using 800 nm Ti:sapphire fs lasers and long mid-infrared lasers also involve laser–matter interaction in the TI regime, the long plateau of harmonics again limits the ER and hence the monochromaticity of the generated XUV. Up to now, there did not exist a method to increase the ER and intensity of the single RH. To take a step ahead in finding a solution to this problem, we note that RH in the MPI regime has not been investigated up to now. Although a few past experiments on HHG from LAP were performed with shorter UV laser wavelengths, thereby resulting in conditions for the MPI regime, RHs were not observed [22], and thus they remain unexplored for this regime of interaction.

In this Letter, we generate for the first time, to our knowledge, the RH in the MPI regime and observe that one could obtain an intense RH with a superior monochromaticity by operating at higher values of the Keldysh parameter. This, in other words, implies that for a given laser intensity, by using driving lasers with shorter wavelengths and hence by increasing the Keldysh parameter, one could increase the ER. This increase in the ER is qualitatively reproduced through numerical simulations based on the three-dimensional time-dependent Schrödinger equation (3D-TDSE) with a model potential. We reveal that Ga^+ from the gallium LAP source driven by 400 nm fs laser pulses ($I_p = 20.52$ eV, $U_p = 2.39$ eV, $\gamma = 2.07$) generates an intense single RH close to 21.9 eV having the potential of multimicrojoule energy, with an unprecedented ER of 714. Our compact, intense XUV source can be integrated into any setup requiring QM-XUV radiation without XUV monochromator installation, preventing

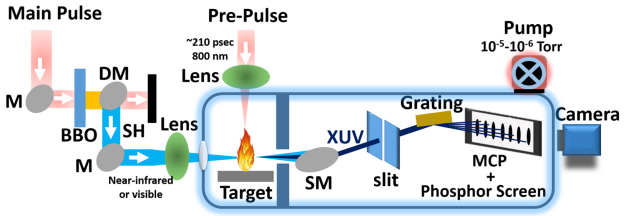

Fig. 1. Schematic diagram of the experimental setup for the HHG from LAP. M, mirror; DM, dichroic mirror; SH, second harmonic; SM, silicon mirror; MCP, microchannel plate.

a substantial loss of XUV flux (typically > 70%) due to the finite diffraction efficiency of the grating monochromator [16].

The schematic diagram of the experimental setup for the HHG from LAP is shown in Fig. 1. The output of an amplified Ti:sapphire laser system (210 ps, 100 Hz, 800 nm) is split into two beams using a 30/70 beam splitter. The 30% part of the beam, called the prepulse, is focused onto a solid target (mounted on an XYZ translation stage) with prepulse energy adjusted to 1.0 mJ, creating an intensity of 1.1×10^{10} W cm^{-2} at the solid target surface for LAP formation. The optical delay between prepulse and main pulse at the solid target was kept at 55 nsec, providing the maximum XUV flux with experiments using a gallium target. The 70% beam, called the main pulse, is compressed down to 40 fs using a dual-grating compressor, and is used to drive the optical parametric amplifier (OPA, TOPAS-800) for frequency conversion. The OPA is parametrically amplified, achieving up to 10 mJ of pulse energy at 1800 nm laser wavelength and can be tuned in the range between 1600 and 2000 nm. See Ref. [23] for the detailed description of the laser source we used for the experiments. The parametrically amplified tunable mid-infrared output of the OPA is frequency-doubled using a BBO crystal (1 mm thick, Type I). The generated near-infrared laser pulses with a pulse duration of 40 fs and pulse energy of 1.5 mJ are focused onto the LAP at an intensity of 1.7×10^{14} W cm^{-2}. For an experiment using 400 nm laser pulses, the compressed 800 nm output of the Ti:sapphire laser is frequency-doubled using a BBO crystal (1 mm thick, Type I) and separated from the collinear 800 nm laser wavelength using a dichroic mirror, generating 400 nm laser pulses with a pulse duration of 57 fs and pulse energy of 1.3 mJ. The main-pulse spot diameter at the focus position is imaged and measured to be 40 μm for the 400 nm and 100 μm for the 860 nm laser wavelength. The generated XUV pulse and copropagating driving laser pulse are split using a silicon mirror placed at a Brewster angle of the main pulse, thereby reflecting only the XUV pulse into the XUV spectrometer. The XUV is frequency-dispersed by the XUV spectrometer comprising a fixed vertical slit, a cylindrical flat-field XUV grating (Hitachi, 1200 lines/mm), a microchannel plate, and a phosphor screen. The harmonics are captured using a 16-bit CMOS camera (model PCO-edge, PCO AG, Germany). The solid target, silicon mirror, and XUV spectrometer are kept inside a vacuum of 10^{-5}–10^{-6} torr.

Figure 2 shows the HHG spectra generated using different near-infrared laser wavelengths driving the gallium LAP. The laser focus was kept 12.3 mm after the LAP, which was the optimal position generating maximum XUV flux at given experimental conditions. The laser spot diameter at the plume is 168 μm, creating an intensity of 1.7×10^{14} W cm^{-2}. The Ga^+ ($I_p = 20.52$ eV) exhibits a strong resonance in the photoionization cross section, with a magnitude of 300 Mbar centered at 21.9 eV, corresponding to

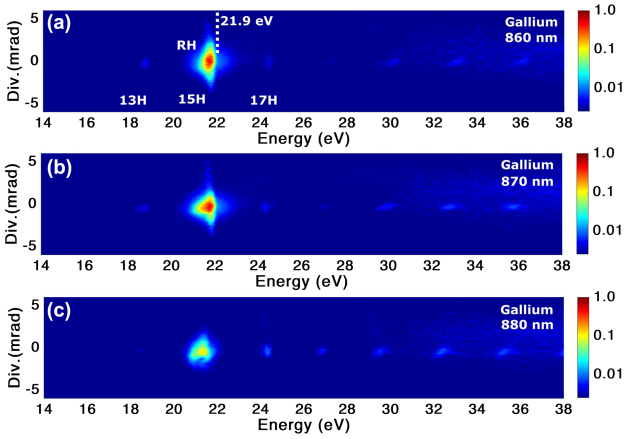

Fig. 2. HHG spectra generated from Ga^+, using (a) 860 nm, (b) 870 nm, and (c) 880 nm laser wavelength. The laser intensity used to generate each harmonic spectrum is 1.7×10^{14} W cm^{-2}.

the strong radiative transition $3d^{10}4s^{2\,1}S_0 \rightarrow 3d^9 4s^2 4p\,^3P_1$ (see Supplement 1 for discussion of the notation) [24]. The Keldysh parameter at 860 nm is 0.935. The state $3d^9 4s^2 4p\,^3P_1$ corresponds to the autoionizing state (AIS) of Ga^+ and the electronic transition from AIS into the ground state $3d^{10}4s^{2\,1}S_0$ is resonant with 15 photons of 860 nm laser field. It is expected that an enhancement or resonance in the photoionization cross section can result in an increase in the harmonic intensity at resonant photon energy [25], and we see an intense RH at the 15th harmonic (15H).

In this work, we define the experimentally observed ER for the RH with the equation $\mathrm{ER} = 2I_q/(I_{q-2} + I_{q+2})$, where I_q is the integrated intensity of RH having order q. At 860 nm laser wavelength, the ER observed is 136. The intensity of 15H decreases as the laser wavelength increases to 870 nm and 880 nm, due to increased off-resonance from the strong radiative transition at 21.9 eV.

To investigate the response of RH from Ga^+ at higher Keldysh parameters, we used a shorter driving laser wavelength of 400 nm. Figure 3(a) shows the intense RH observed at a laser intensity of 1.6×10^{14} W cm^{-2}, with laser focus kept 10.1 mm after the LAP. The laser spot diameter at the plume is 135 μm. The 21.9 eV resonance is seven-photon resonant with the 400 nm driving laser photon, generating an intense 7H. The value of U_p and I_p is 2.39 eV and 20.52 eV, respectively, resulting in a Keldysh parameter of 2.07. The I_p is more than 8 times higher compared to the U_p, and RH is generated in the MPI regime. The peak intensity of RH from Ga^+ with 400 nm laser wavelength is observed to be 4.5 times stronger than the RH with 860 nm laser wavelength, stronger due to the low number of laser photons required for resonance with the AIS using the former wavelength.

We summarize in Table 1 the ER obtained experimentally using 400 and 860 nm laser wavelengths. The ER observed using 400 nm laser wavelength is 714. The highest ER value reported so far is from indium LAP, generating an intense RH with an ER of ∼100 [18]. Therefore, the ER of 714 observed in our experiment under the MPI regime is the highest value reported so far using the LAP technique, making gallium LAP a source of intense RH with unprecedented monochromaticity from a high-order harmonic source. The FWHM bandwidth of the generated 21.9 eV RH is 0.28 eV, which is broad enough to support a 6.5 fs pulse duration for a Fourier-transform limited pulse.

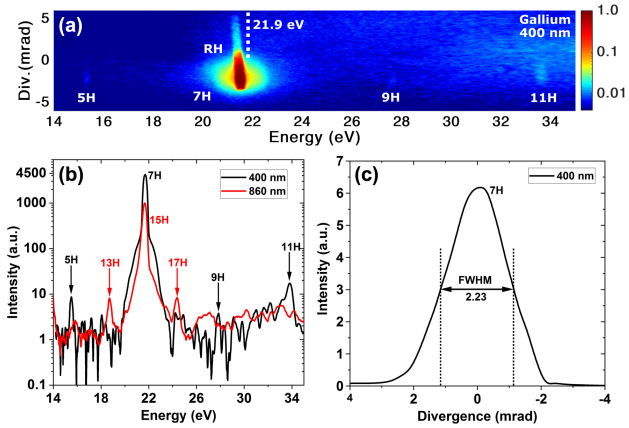

Fig. 3. HHG spectra generated from Ga^+, using (a) 400 nm laser wavelength; (b) vertically integrated line profile of RH from Ga^+ using 400 nm and 860 nm laser wavelength; (c) FWHM divergence of RH is 2.23 mrad, indicating the coherent nature of RH emission. The laser intensity used to generate harmonic spectrum at 400 nm and 860 nm wavelength is 1.6×10^{14} W cm^{-2} and 1.7×10^{14} W cm^{-2}, respectively.

Table 1. Experimentally Observed and Calculated ER Values Using 3D-TDSE from Ga^+

Experiment			
Laser Wavelength (nm)	**Laser Intensity (W cm^{-2})**	**Keldysh Parameter**	**ER**
860	1.7×10^{14}	0.935	136
400	1.6×10^{14}	2.07	714
Calculated			
Laser Wavelength (nm)	**Laser Intensity (W cm^{-2})**	**Keldysh Parameter**	**ER**
850	5×10^{14}	0.55	71
400	5×10^{14}	1.17	352
850	3×10^{14}	0.71	103
400	3×10^{14}	1.51	633

The calculated ER using 3D-TDSE with a model potential, reproducing the I_p and AIS energy in Ga^+, is also shown in Table 1. The details of the calculations are given in Supplement 1. The calculations show that a superior ER can be achieved by increasing the Keldysh parameter, qualitatively in agreement with the experiments.

The RH intensity from gallium LAP was compared with other LAPs known to generate intense harmonics, such as the graphite LAP that has previously demonstrated intense multimicrojoule energies in each harmonic order in the XUV region [26–28], and tin LAP, demonstrating intense RH with 10^{-4} efficiency [29]. As seen in the Supplement 1 Fig. S.3, we found that Ga^+ driven with 400 nm laser wavelength at similar laser intensities results in the RH peak intensity that is twice the harmonic intensity from graphite LAP and 3.3 times higher than the tin RH. Since previous studies have reported 1.1 μJ of RH pulse energy for tin at 10^{-4} level conversion efficiency [29], the relative comparison of RH intensity of Ga^+ establishes it as a potential source of intense QM-XUV with multimicrojoule pulse energy.

In the TI regime, the mechanism of RH generation for most materials can be explained by the four-step model [30]. The first two steps of this model are the same as the three-step model, i.e.,

TI of the valence electron and its acceleration within the continuum [30]. The third step, however, involves resonant capture of the tunnel-ionized electron into the AIS, i.e., a discrete state embedded in the continuum, which is followed by the fourth step involving a radiative transition from AIS to the initial ground state emitting RH [30–32]. The RH generation mechanism in the MPI regime can be similar to the four-step model applicable for RH generation in the TI regime, incorporating multiphoton resonant up-transition from the ground state into the AIS, instead of capturing of the tunnel-ionized electron by AIS in the continuum. The radiative one-photon down-transition from AIS into the ground state will emit XUV with intensity proportional to the down-transition amplitude. This will essentially form a two-step model with the inclusion of AIS [33–35]. The TDSE calculations reveal that the higher RH intensity and ER in the MPI regime relative to the TI regime could be attributed to the electron wave packet spreading after photoionization in the TI regime (see Section 3 of Supplement 1 for more details). The wave packet spreads at the second step of the four-step model, which populates AIS with relatively low probability; this spreading is absent in the MPI regime, where AIS is populated directly from the ground state. The temporal coherence of the RH emission can be related to the very short lifetime of AIS $3d^9 4s^2 4p\ ^3P_1$ involved, which can be retrieved from the corresponding linewidth. The AIS linewidth is $\Gamma = 142$ meV (see Supplement 1), resulting in a very short lifetime of $\tau \sim 4.6$ fs $(\hbar/\Gamma)$.

In conclusion, we have demonstrated for the first time in the MPI regime, a compact, intense QM-XUV source based on HHG using the LAP technique. We observe an increase in the ER with an increased Keldysh parameter, which shows that the use of short wavelength lasers results in an intense RH with superior ER. This will pave the way to find further methods to completely suppress the nonresonant harmonics, generating only the single RH free of other nonresonant harmonics, which are typically observed as a long harmonic plateau in the TI regime. The increase in ER is qualitatively reproduced through numerical simulations based on 3D-TDSE. The gallium LAP driven by a 400 nm laser demonstrates an unprecedented ER of 714 delivered without any monochromator installation, hence preventing a substantial loss of XUV flux. Given that at the present time, the amplified Ti:sapphire laser sources with energies >1 Joule per pulse are available, the excellent monochromaticity shown by the LAP-based XUV source with 10^{-4} level conversion efficiency could also enable us to aim for the submillijoule table-top fs XUV sources in the future. The new observation of RH in the MPI regime will also motivate further theoretical studies for a better understanding of the dynamics of AIS and its role in the mechanism of RH generation in the previously unexplored MPI regime of laser–matter interaction.

Funding. Russian Foundation for Basic Research (19-02-00739); Foundation for the Advancement of Theoretical Physics and Mathematics; Mitacs.

Disclosures. The authors declare no conflicts of interest.

Data availability. Data underlying the results presented in this paper are not publicly available at this time but may be obtained from the authors upon reasonable request.

Supplemental document. See Supplement 1 for supporting content.

REFERENCES

1. C. Winterfeldt, C. Spielmann, and G. Gerber, Rev. Mod. Phys. **80**, 117 (2008).
2. R. A. Ganeev, J. Phys. B **40**, R213 (2007).
3. P. B. Corkum, Phys. Rev. Lett. **71**, 1994 (1993).
4. J. Itatani, J. Levesque, D. Zeidler, H. Niikura, H. Pépin, J. C. Kieffer, P. B. Corkum, and D. M. Villeneuve, Nature **432**, 867 (2004).
5. H. J. Wörner, J. B. Bertrand, D. V. Kartashov, P. B. Corkum, and D. M. Villeneuve, Nature **466**, 604 (2010).
6. F. Kelkensberg, C. Lefebvre, W. Siu, O. Ghafur, T. T. Nguyen-Dang, O. Atabek, A. Keller, V. Serov, P. Johnsson, M. Swoboda, T. Remetter, A. L'Huillier, S. Zherebtsov, G. Sansone, E. Benedetti, F. Ferrari, M. Nisoli, F. Lépine, M. F. Kling, and M. J. J. Vrakking, Phys. Rev. Lett. **103**, 123005 (2009).
7. A. Ravasio, D. Gauthier, F. R. N. C. Maia, M. Billon, J.-P. Caumes, D. Garzella, M. Géléoc, O. Gobert, J.-F. Hergott, A.-M. Pena, H. Perez, B. Carré, E. Bourhis, J. Gierak, A. Madouri, D. Mailly, B. Schiedt, M. Fajardo, J. Gautier, P. Zeitoun, P. H. Bucksbaum, J. Hajdu, and H. Merdji, Phys. Rev. Lett. **103**, 028104 (2009).
8. E. J. Sie, T. Rohwer, C. Lee, and N. Gedik, Nat. Commun. **10**, 3535 (2019).
9. O. Schmidt, M. Bauer, C. Wiemann, R. Porath, M. Scharte, O. Andreyev, G. Schönhense, and M. Aeschlimann, Appl. Phys. B **74**, 223 (2002).
10. A. Nayak, I. Orfanos, I. Makos, M. Dumergue, S. Kühn, E. Skantzakis, B. Bodi, K. Varju, C. Kalpouzos, H. I. B. Banks, A. Emmanouilidou, D. Charalambidis, and P. Tzallas, Phys. Rev. A **98**, 023426 (2018).
11. K. Midorikawa, Y. Nabekawa, and A. Suda, Prog. Quantum Electron. **32**, 43 (2008).
12. C. Pellegrini, A. Marinelli, and S. Reiche, Rev. Mod. Phys. **88**, 015006 (2016).
13. R. W. Schoenlein, S. Chattopadhyay, H. H. W. Chong, T. E. Glover, P. A. Heimann, C. V. Shank, A. A. Zholents, and M. S. Zolotorev, Science **287**, 2237 (2000).
14. S. Khan, K. Holldack, T. Kachel, R. Mitzner, and T. Quast, Phys. Rev. Lett. **97**, 074801 (2006).
15. R. A. Ganeev, L. B. E. Bom, and T. Ozaki, Appl. Phys. Lett. **91**, 131104 (2007).
16. L. Poletto, P. Villoresi, E. Benedetti, F. Ferrari, S. Stagira, G. Sansone, and M. Nisoli, J. Opt. Soc. Am. B **25**, B44 (2008).
17. T. Ditmire, J. K. Crane, H. Nguyen, L. B. DaSilva, and M. D. Perry, Phys. Rev. A **51**, R902 (1995).
18. R. A. Ganeev, M. Suzuki, M. Baba, H. Kuroda, and T. Ozaki, Opt. Lett. **31**, 1699 (2006).
19. C. Hutchison, R. A. Ganeev, T. Witting, F. Frank, W. A. Okell, J. W. G. Tisch, and J. P. Marangos, Opt. Lett. **37**, 2064 (2012).
20. G. S. Boltaev, V. V. Kim, M. Iqbal, N. A. Abbasi, V. S. Yalishev, R. A. Ganeev, and A. S. Alnaser, Photonics **7**, 66 (2020).
21. J.-F. Hergott, M. Kovacev, H. Merdji, C. Hubert, Y. Mairesse, E. Jean, P. Breger, P. Agostini, B. Carré, and P. Salières, Phys. Rev. A **66**, 021801 (2002).
22. Y. Akiyama, K. Midorikawa, Y. Matsunawa, Y. Nagata, M. Obara, H. Tashiro, and K. Toyoda, Phys. Rev. Lett. **69**, 2176 (1992).
23. N. Thiré, S. Beaulieu, V. Cardin, A. Laramée, V. Wanie, B. E. Schmidt, and F. Légaré, Appl. Phys. Lett. **106**, 091110 (2015).
24. B. Peart, I. C. Lyon, and K. Dolder, J. Phys. B **20**, 5403 (1987).
25. M. A. Fareed, V. V. Strelkov, M. Singh, N. Thiré, S. Mondal, B. E. Schmidt, F. Légaré, and T. Ozaki, Phys. Rev. Lett. **121**, 023201 (2018).
26. L. B. E. Bom, Y. Pertot, V. R. Bhardwaj, and T. Ozaki, Opt. Express **19**, 3077 (2011).
27. M. A. Fareed, N. Thiré, S. Mondal, B. E. Schmidt, F. Légaré, and T. Ozaki, Appl. Phys. Lett. **108**, 124104 (2016).
28. M. Singh, M. A. Fareed, A. Laramée, E. Isgandarov, and T. Ozaki, Appl. Phys. Lett. **115**, 231105 (2019).
29. M. Suzuki, M. Baba, R. Ganeev, H. Kuroda, and T. Ozaki, Opt. Lett. **31**, 3306 (2006).
30. V. Strelkov, Phys. Rev. Lett. **104**, 123901 (2010).
31. V. V. Strelkov, M. A. Khokhlova, and N. Y. Shubin, Phys. Rev. A **89**, 053833 (2014).
32. M. A. Fareed, V. V. Strelkov, N. Thiré, S. Mondal, B. E. Schmidt, F. Légaré, and T. Ozaki, Nat. Commun. **8**, 16061 (2017).
33. J. M. N. Djiokap and A. F. Starace, Phys. Rev. A **88**, 053412 (2013).
34. J. M. N. Djiokap and A. F. Starace, Phys. Rev. A **102**, 013103 (2020).
35. A. I. Magunov and V. V. Strelkov, Phys. Wave Phenomena **28**, 369 (2020).